Vibrations and reorientations of H2O molecules in [Sr(H2O)(6)]Cl-2 studied by Raman light scattering, incoherent inelastic neutron scattering and proton magnetic resonance

ARTICLE *in* SPECTROCHIMICA ACTA PART A MOLECULAR AND BIOMOLECULAR SPECTROSCOPY · JANUARY 2014

Impact Factor: 2.35 · DOI: 10.1016/j.saa.2014.01.054 · Source: PubMed

6 AUTHORS, INCLUDING:

Edward Mikuli
Jagiellonian University
98 PUBLICATIONS **639** CITATIONS
SEE PROFILE

Małgorzata Florek-Wojciechowska
University of Warmia and Mazury in Olsztyn
3 PUBLICATIONS **0** CITATIONS
SEE PROFILE

Spectrochimica Acta Part A: Molecular and Biomolecular Spectroscopy 124 (2014) 429–440

Contents lists available at ScienceDirect

Spectrochimica Acta Part A: Molecular and Biomolecular Spectroscopy

journal homepage: www.elsevier.com/locate/saa

Vibrations and reorientations of H_2O molecules in $[Sr(H_2O)_6]Cl_2$ studied by Raman light scattering, incoherent inelastic neutron scattering and proton magnetic resonance

Joanna Hetmańczyk [a,b,*], Łukasz Hetmańczyk [a,b], Anna Migdał-Mikuli [a], Edward Mikuli [a], Małgorzata Florek-Wojciechowska [c], Hubert Harańczyk [c]

[a] Jagiellonian University, Faculty of Chemistry, Ingardena 3, 30-060 Kraków, Poland
[b] Frank Laboratory of Neutron Physics, JINR, Dubna 141980, Russia
[c] Institute of Physics, Jagiellonian University, ul. Reymonta 4, 30-059 Kraków, Poland

HIGHLIGHTS

- Calculated FT-IR, Raman and neutron scattering spectra compared with experimental results.
- Molecular reorientations in $[Sr(H_2O)_6]Cl_2$ at phase transition studied by RS.
- Dynamics of H_2O ligands is disturbed in the phase transition.
- ^1H NMR results revealed two kinds structurally not equivalent water molecules in the crystal lattice $[Sr(H_2O)_6]Cl_2$.

GRAPHICAL ABSTRACT

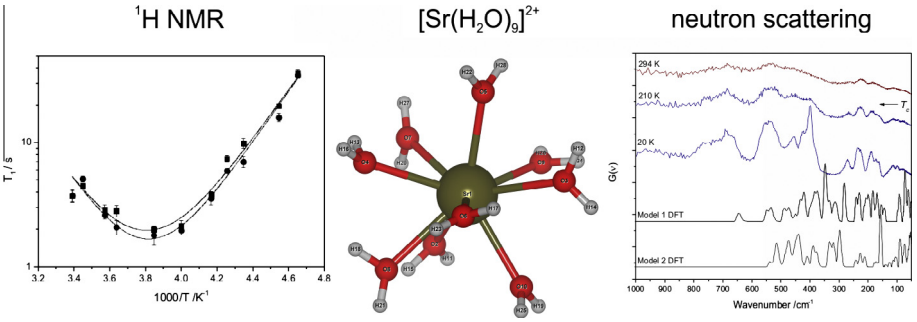

ARTICLE INFO

Article history:
Received 1 October 2013
Received in revised form 4 January 2014
Accepted 10 January 2014
Available online 21 January 2014

Keywords:
Hexaaquastrontium chloride
Crystal structure and molecular reorientations
Raman scattering (RS)
Neutron powder diffraction (NPD)
Inelastic and quasielastic incoherent neutron scattering (IINS and QENS)
Proton magnetic resonance (^1H NMR)

ABSTRACT

Vibrational–reorientational dynamics of H_2O ligands in the high- and low-temperature phases of $[Sr(H_2O)_6]Cl_2$ was investigated by Raman Spectroscopy (RS), proton magnetic resonance (^1H NMR), quasielastic and inelastic incoherent Neutron Scattering (QENS and IINS) methods. Neutron powder diffraction (NPD) measurements, performed simultaneously with QENS, did not indicated a change of the crystal structure at the phase transition (detected earlier by differential scanning calorimetry (DSC) at $T_C^h = 252.9$ K (on heating) and at $T_C^c = 226.5$ K (on cooling)). Temperature dependence of the full-width at half-maximum (FWHM) of ν_s(OH) band at ca. 3248 cm^{-1} in the RS spectra indicated small discontinuity in the vicinity of phase transition temperature, what suggests that the observed phase transition may be associated with a change of the H_2O reorientational dynamics. However, an activation energy value (E_a) for the reorientational motions of H_2O ligands in both phases is nearly the same and equals to ca. 8 kJ mol^{-1}. The QENS peaks, registered for low temperature phase do not show any broadening. However, in the high temperature phase a small QENS broadening is clearly visible, what implies that the reorientational dynamics of H_2O ligands undergoes a change at the phase transition. ^1H NMR line is a superposition of two powder Pake doublets, differentiated by a dipolar broadening, suggesting that there are two types of the water molecules in the crystal lattice of $[Sr(H_2O)_6]Cl_2$ which are structurally not equivalent average distances between the interacting protons are: 1.39 and 1.18 Å. However, their reorientational dynamics is very similar ($\tau_c = 3.3 \cdot 10^{-10}$ s). Activation energies for the reorientational motion of these both kinds of H_2O ligands have nearly the same values in an experimental error limit: and equal to ca. 40 kJ mole^{-1}. The phase transition is not seen in the ^1H NMR spectra temperature dependencies. Infrared (IR), Raman

* Corresponding author at: Jagiellonian University, Faculty of Chemistry, Ingardena 3, 30-060 Kraków, Poland. Tel.: +48 12 633 2265; fax: +48 12 634 0515.
E-mail address: serwonsk@chemia.uj.edu.pl (J. Hetmańczyk).

1386-1425/$ - see front matter
http://dx.doi.org/10.1016/j.saa.2014.01.054

(RS) and inelastic incoherent neutron scattering (IINS) spectra were calculated by the DFT method and quite a good agreement with the experimental data was obtained.

Introduction

Hexaaquastrontium chloride, with formula $[Sr(H_2O)_6]Cl_2$, is a particularly interesting molecular material because of occurrence of phase transition and fast reorientational motions of the H_2O ligands. At room temperature, (*RT*), hexaaquastrontium chloride crystallises in the trigonal system (P321 space group, No = 150) with unit cell parameter: $a = b = 7.9596$ Å, $c = 4.1243$ Å and one molecule per unit cell. There are two kinds o water molecules: H(1)-O(1)–H(1) and H(2)–O(2)–H(2), which are coordinated differently to Sr^{2+} cations. Each O(1) adjoining only one Sr^{2+} and each O(2) shared between two Sr^{2+} cations. Thus, there are two different metal–oxygen distances: Sr–O(1) = 2.570 and Sr–O(2) = 2.715 Å [1]. The ninefold coordination polyhedron can be described with six O(2) and three O(1) atoms. Exists a helical system of hydrogen bonding involves three H(1) and three H(2) atoms (arising from these two kinds of water molecules), and the Cl^- anions [2]. Each of Cl^- anion takes part in three of these bonding systems, thus forming six hydrogen bonds. The crystal structure of $[Sr(H_2O)_6]Cl_2$ is consistent with earlier X-ray diffraction studies [2,3] and it is isostructural (isotopic) with $[Ca(H_2O)_6]Cl_2$ [4]. Spectroscopic studies [5,6] also confirm that $[Sr(H_2O)_6]Cl_2$ includes two sets of differently bonded, but not much distorted H_2O molecules.

We have studied the melting and thermal decomposition of $[Sr(H_2O)_6]Cl_2$ using thermal gravimetric analysis (TGA) and differential scanning calorimetry (DSC) [7]. The gaseous products of the title compound's decomposition process were identified online by a quadruple mass spectrometer (QMS). The thermal decomposition of the title compound proceeds in two main stages. In first stage dehydration of hexaaquastrontium chloride to strontium chloride undergoes in three steps and all (2/6, 3/6 and 1/6) of H_2O molecules are liberated. In the second stage the investigated anhydrous $SrCl_2$ remains unchanged up to ca. 900 K.

The phase transition of $[Sr(H_2O)_6]Cl_2$ was detected using differential scanning calorimetry (DSC), Fourier transform middle and far infrared absorption (FT-MIR and FT-FIR) spectroscopes [7]. One phase transition (PT) at $T_C^h = 252.9$ K (on heating) and at $T_C^c = 226.5$ K (on cooling) was detected by DSC for $[Sr(H_2O)_6]Cl_2$ in 123–295 K range. Thermal hysteresis of this PT is relatively large and equals to 26.4 K. Entropy change (ΔS) value at this first-order type phase transition equals to ca. 1.5 J mol^{-1} K^{-1}. The temperature dependences of the full width at half maximum (FWHM) values of the infrared bands associated with $\rho_t(H_2O)E$ and $\delta_{as}(HOH)E$ modes (at ca. 417 and 1628 cm^{-1}, respectively) suggest that the observed phase transition is associated with a sudden change of a speed of the H_2O reorientational motions. The H_2O ligands in the high temperature phase reorientate fast (correlation times 10^{-11}–10^{-13} s) with the activation energy of ca. 2 kJ mol^{-1}. Below T_C^c probably a part of the H_2O ligands stopped their fast reorientation, while the remainders continued their fast reorientation, but with the activation energy of ca. 8 kJ mol^{-1}. Far and middle infrared spectra indicated characteristic changes at the vicinity of PT with decreasing of temperature, which suggested lowering of the crystal structure symmetry. Splitting of the band connected with $\nu_{as}(OH)$ mode (at ca. 3600 cm^{-1}) near the T_C^c suggested lowering of the crystal lattice symmetry. All these facts suggest that the discovered PT is connected both with a change of the reorientational dynamics of the H_2O ligands and with a change of the crystal structure [7].

The aim of the present study is to find connections between the previously recorded phase transition [7] and eventual changes in the rate of stochastic reorientational motions of the H_2O ligands and/or of the crystal structure, by means of Raman light scattering (RS), inelastic/quasi-elastic incoherent neutron scattering (IINS/QENS) and neutron powder diffraction (NPD) methods. IINS/QENS methods may inform us about fast (correlation time τ_c: 10^{-12}–10^{-13} s) reorientational molecular motions. NPD method can find the connection of PT with the changes in the crystal structure. We would like also to compare the results obtained by the Raman scattering spectroscopy with the data obtained earlier [7] by Fourier transform middle and far-infrared spectroscopy (FT-MIR and FT-FIR). We hope that these studies make it possible to obtain more precise picture of the phase polymorphism of the title compound. Moreover, employed to these investigations also ^{1}H NMR method we would like to confirm additionally the existence of the two kinds of water molecules in $[Sr(H_2O)_6]Cl_2$ which are both structurally and dynamically not equivalent.

Experimental section

The sample of the title compound investigated in the present study was employed earlier in DSC and IR measurements [7]; the details of the synthesis and chemical analysis of the examined compound were also described in that paper.

Raman spectra were recorded on a MultiRAM FT-Raman spectrometer equipped with a 1064 nm laser line (laser power set on 250 mW) and with a germanium detector. All spectra were collected in a 4000–50 cm^{-1} range, with 4 cm^{-1} resolution, and a total of 64 scans were accumulated. The RS spectra were recorded during cooling of the sample across the temperature range of 298–158 K (steps of 10 K). Temperature measurements were performed using the Linkam THMSG600 heating and freezing stage. Temperature accuracy was equal to 0.1 °C.

The incoherent inelastic/quasielastic neutron scattering spectra were measured using the time-of-flight method on a NERA spectrometer [8] at the high flux pulsed reactor IBR-2M in Dubna (Russia) at temperatures of $T = 20$, 210 and 294 K. A sample with a mass of ca. 10 g was loaded at room temperature into a flat thin-walled aluminium container, which was placed in a top-loaded cryostat cooled using a helium refrigerator. The neutron flux passed through a $5 \times 15 = 75$ cm^2 sample area. The neutron transmission was ca. 80%. The temperature of the sample could be changed within the range 20–300 K and stabilised with ±0.5 K accuracy at any chosen value. The energy resolution of the NERA spectrometer amounted to ca. 3% for the IINS spectra in the range of 1000–100 cm^{-1}. The energy of incoming neutrons was analysed by time of flight (TOF) of the 110 m flight path from the reactor to the sample position. The energy of scattered neutrons was equal to 4.58 meV (neutrons were monochromatised using Bragg scattering from pyrolytic graphite). IINS measurements were made for several scattering angles. The final IINS spectra were obtained by summing up the data taken from all 15 detectors covering scattering angles from 20° to 160°. The obtained spectra were corrected for scattering of the aluminium sample holder (Al). The linear background coming from fast neutrons was also subtracted. The IINS data were not corrected for the multi-scattering process, because of the low thickness of the sample and high transmission. The registered QENS spectra were treated qualitatively. The instrument resolution was low, so the QENS broadening was not readily

separable from the elastic component for particular detectors. Moreover, data coming from detectors positioned at high angles were strongly affected by diffraction peaks. During the data processing these peaks were manually removed (i.e. points lying between the start and the end of the particular diffraction peak were cut) but this procedure undoubtedly introduced some errors. The shape of QENS data were distorted by the Be filter's cutoff edge. Neutron powder diffraction (NPD) patterns were measured simultaneously with the IINS/QENS spectra. In the case of the NPD, different scattering angles were used to record the selected lattice spacing d_{hkl} ranges at an appropriate resolution. It should be emphasised that, because the examined compound contained hydrogen atoms, the NPD patterns were recorded against a relatively high incoherent background, due to the incoherent scattering cross-section of hydrogen atoms. For this reason, their interpretation is only qualitative, but nevertheless very useful for identification of the particular phases.

^{1}H NMR spectra were collected on Bruker Avance III spectrometer (Bruker Biospin), operating at the resonance frequency 300 MHz (at $B_0 = 7$ T), with the transmitter power used equal to 400 W. The pulse length was $\pi/2 = 2.1$ μs, bandwidths 500 kHz, and repetition time was no shorter than 40 s (and was set equal to the longest τ in the given experiment). The relaxation spectroscopy experiment was performed using the inversion recovery sequence (π–τ–$\pi/2$), with the delay time τ ranged between 1 ms and 120 s. Every recorded spectrum was averaged over 16 accumulations. The sample was cooled from 297 K down to 215 K and the temperature was stabilized in a gaseous nitrogen stream, with an accuracy of ±0.1 K.

Computational details

The main goal of these calculations was to obtain harmonic vibrational frequencies, which could be used to support the interpretation of the experimental spectra. The optimization of the geometry and frequency calculations were carried out with Gaussian 09 package, Revision C.01 [9], implemented on the ZEUS computer in the Academic Computer Centre, Cyfronet AGH, Kraków. The calculations were performed for two models: the first (named as Model 1) was based on the isolated equilibrium model of single $[Sr(H_2O)_9]^{2+}$ whereas in the second (Model 2) we choose two Sr atoms surrounded by 9 H_2O ligands and also two Cl^- anions were incorporated: $[Sr_2(H_2O)_9Cl_2]^{2+}$. The initial geometries for both models were derived from the crystallographic data for the high-temperature phase [1]. The calculations were carried out on the basis of density functional theory (DFT), using three-parameter hybrid functional B3LYP, which combines the Becke's gradient-corrected (GGA) exchange functional and the Lee–Yang–Parr and Vosko–Wilk–Nusair correlation functionals with the 20% part of the exact Hartree–Fock exchange energy [10,11]. The basis set LANL2DZ ECP, with effective core potential (ecp) was set on the strontium atom [12,13] while the extended Pople-type 6-311 + G(d,p) basis set was set on the water ligands.

Computed Raman activities were transformed into theoretical Raman intensities using the following expression:

$$I_i = 10^{-12} \times (v_0 - v_i)^4 \times (1/v_i) \times \mathrm{RA}_i, \quad (1)$$

where I_i is the Raman intensity, RA_i is the Raman scattering activities, v_i is the wavenumber of the normal modes, and v_0 denotes the wavenumber of the light of excitation laser (in our measurements $v_0 = 1064$ nm = 9398.5 cm^{-1}) [14]. The theoretical intensities were convoluted with Lorentzian function. The widths of bands in the presented calculated spectra were fitted to the experimental spectra.

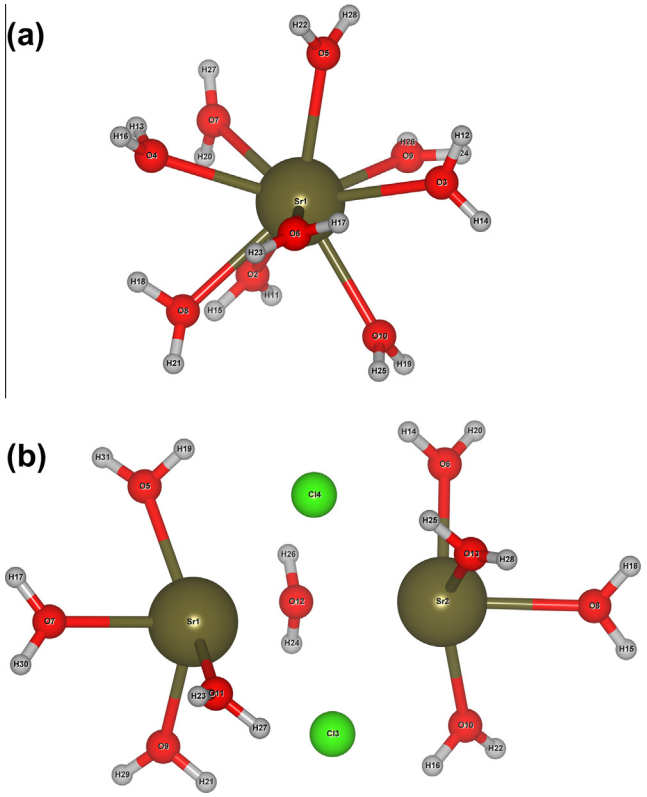

Fig. 1. Equilibrium geometry of: (a) $[Sr(H_2O)_9]^{2+}$ cation (Model 1) and (b) $[Sr_2(H_2O)_9Cl_2]^{2+}$ (Model 2) used in DFT calculation.

Results and discussion

Molecular structure and vibrational spectra

The equilibrium geometries computed with B3LYP/LANL2DZ ECP/6-311 + G(d,p) level of theory are shown in Fig. 1a and b for Model 1 and 2, respectively. Model 1 belongs to the C_s point group, possessing only σ mirror plane, whereas Model 2 has the C_2 point group. The symmetry is in agreement with the high-temperature crystalline phase [1].

In the crystal structure of $[Sr(H_2O)_6]Cl_2$ hydrogen bonds exist. In our simple model employed in the calculation the hydrogen bond interactions were not introduced (modelled) and thus were not taken into account. It should be remembered that differences in the structure of the intra-molecular hydrogen bond system obtained may affect the theoretical spectra, especially in the spectral range connected with the librational modes of hydrated water. The hydrogen bonds sequence is sensitive to the geometry of these bonds [15]. A comparison between experimental and calculated values is presented in Table 1 for Model 1 and in Table 2 for Model 2, respectively. The atomic labelling sequence used in these studies is shown in Fig. 1a and b. Harmonic frequency calculations confirmed that the obtained geometry is the real minimum on the Potential Energy Surface (PES). The Model 1 gives a better approximation of experimental geometry than Model 2. The O–H bond lengths as well as Sr–O bond lengths are reproduced well. Small expansion of the calculated Model 1 geometry with respect to experimental structure can be noticed. Some of the Sr–O bonds are elongated. This can be explained as follows. In real crystal the atoms are surrounded by more than one shell (unit cell packing) formed by other atoms. Hence forces acting on atoms in one chosen unit cell and coming from the atoms in surroundings cells are responsible for contraction of the structure. The distribution

Table 1
The comparison of experimental and calculated for Model 1 bonds lengths for $[Sr(H_2O)_6]Cl_2$.

Experimental		Calculated model 1	
Bond	Length (A)	Bond	Length (A)
Sr(1)_O(2)	2.715	Sr(1)_O(2)	2.7902
Sr(1)_O(3)	2.715	Sr(1)_O(3)	2.7583
Sr(1)_O(4)	2.715	Sr(1)_O(4)	2.7900
Sr(1)_O(5)	2.715	Sr(1)_O(5)	2.7153
Sr(1)_O(6)	2.570	Sr(1)_O(6)	2.6715
Sr(1)_O(7)	2.570	Sr(1)_O(7)	2.7928
Sr(1)_O(8)	2.715	Sr(1)_O(8)	2.7928
Sr(1)_O(9)	2.570	Sr(1)_O(9)	2.6716
Sr(1)_O(10)	2.715	Sr(1)_O(10)	2.7150
O(2)_H(11)	0.967	O(2)_H(11)	0.9649
O(2)_H(15)	0.967	O(2)_H(15)	0.9687
O(3)_H(12)	0.967	O(3)_H(12)	0.9652
O(3)_H(14)	0.967	O(3)_H(14)	0.9652
O(4)_H(13)	0.967	O(4)_H(13)	0.9687
O(4)_H(16)	0.967	O(4)_H(16)	0.9649
O(5)_H(22)	0.967	O(5)_H(22)	0.9653
O(5)_H(28)	0.967	O(5)_H(28)	0.9652
O(6)_H(17)	0.947	O(6)_H(17)	0.9651
O(6)_H(23)	0.947	O(6)_H(23)	0.9647
O(7)_H(20)	0.947	O(7)_H(20)	0.9684
O(7)_H(27)	0.947	O(7)_H(27)	0.9650
O(8)_H(18)	0.967	O(8)_H(18)	0.9683
O(8)_H(21)	0.967	O(8)_H(21)	0.9645
O(9)_H(24)	0.947	O(9)_H(24)	0.9651
O(9)_H(26)	0.947	O(9)_H(26)	0.9647
O(10)_H(19)	0.967	O(10)_H(19)	0.9653
O(10)_H(25)	0.967	O(10)_H(25)	0.9652

The most significant differences for Sr - O and Sr - Cl distances are bolted.

Table 2
The comparison of experimental and calculated for Model 2 bonds lengths for $[Sr(H_2O)_6]Cl_2$.

Experimental		Calculated model 2	
Bond	Length (A)	Bond	Length (A)
Sr(1)_O(5)	2.570	Sr(1)_O(5)	2.629
Sr(1)_O(7)	2.570	Sr(1)_O(7)	2.632
Sr(1)_O(9)	2.570	Sr(1)_O(9)	2.617
Sr(1)_O(11)	2.715	Sr(1)_O(11)	2.607
Sr(1)_O(12)	2.715	Sr(1)_O(12)	2.968
Sr(1)_O(13)	**2.715**	**Sr(1)_O(13)**	**5.210**
Sr(2)_O(11)	**2.715**	**Sr(2)_O(11)**	**5.210**
Sr(2)_O(12)	2.715	Sr(2)_O(12)	2.968
Sr(2)_O(13)	2.715	Sr(2)_O(13)	2.607
Sr(2)_O(6)	2.570	Sr(2)_O(6)	2.617
Sr(2)_O(8)	2.570	Sr(2)_O(8)	2.632
Sr(2)_O(10)	2.570	Sr(2)_O(10)	2.629
Sr(1)_Sr(2)	4.124	Sr(1)_Sr(2)	4.395
Sr(1)_Cl(3)	**4.909**	**Sr(1)_Cl(3)**	**3.095**
Sr(2)_Cl(3)	**5.183**	**Sr(2)_Cl(3)**	**3.053**
Sr(1)_Cl(4)	**5.183**	**Sr(1)_Cl(4)**	**3.053**
Sr(2)_Cl(4)	**4.909**	**Sr(2)_Cl(4)**	**3.095**
O(5)_H(31)	0.947	O(5)_H(31)	0.964
O(5)_H(19)	0.947	O(5)_H(19)	0.971
O(9)_H(21)	0.947	O(9)_H(21)	0.970
O(9)_H(29)	0.947	O(9)_H(29)	0.964
O(7)_H(17)	0.947	O(7)_H(17)	0.965
O(7)_H(30)	0.947	O(7)_H(30)	0.966
O(6)_H(14)	0.947	O(6)_H(14)	0.970
O(6)_H(20)	0.947	O(6)_H(20)	0.964
O(8)_H(15)	0.947	O(8)_H(15)	0.965
O(8)_H(18)	0.947	O(8)_H(18)	0.966
O(10)_H(16)	0.947	O(10)_H(16)	0.971
O(10)_H(22)	0.947	O(10)_H(22)	0.964
O(11)_H(23)	0.967	O(11)_H(23)	0.964
O(11)_H(27)	0.967	O(11)_H(27)	0.970
O(13)_H(25)	0.967	O(13)_H(25)	0.970
O(13)_H(28)	0.967	O(13)_H(28)	0.964
O(12)_H(24)	0.967	O(12)_H(24)	0.967
O(12)_H(26)	0.967	O(12)_H(26)	0.967

The most significant differences for Sr - O and Sr - Cl distances are bolted.

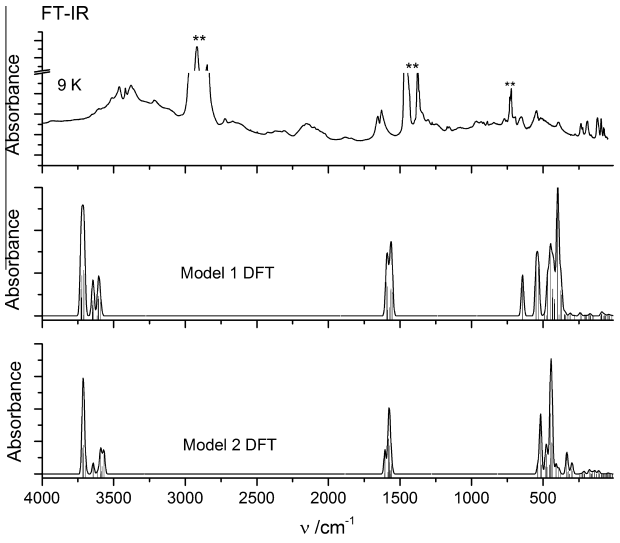

Fig. 2. Calculated (Model 1 and Model 2) and experimental vibrational IR spectra of $Sr(H_2O)_6]Cl_2$ in the range from 4000 to 50 cm^{-1} (∗denotes bands of Nujol). Theoretical spectra were multiplied by scale factor 0.9688.

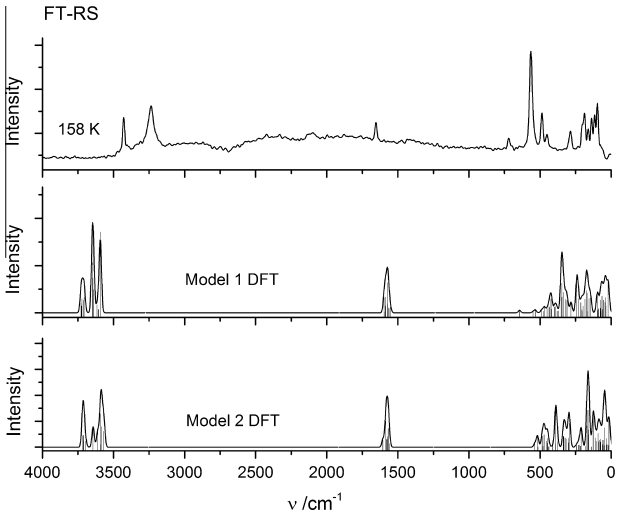

Fig. 3. Calculated (Model 1 and Model 2) and experimental vibrational RS spectra of $Sr(H_2O)_6]Cl_2$ in the range from 4000 to 50 cm^{-1}. Theoretical spectra were multiplied by scale factor 0.9688.

of water molecules is spherical and more resembles the situation found in crystal. The equilibrium structure obtained in case of Model 2 is more distorted in comparison with experimental one. The most significant differences (bolted in Table 2) are observed for Sr–O distances. Water molecules which formed bridge between two Sr atoms in the starting structure were shifted during geometry optimization towards particular Sr atom. The structure has also expanded.

The calculated FT-IR and FT-RS spectra are compared with the experimental spectra in Figs. 2 and 3, respectively. In these figures the computed frequencies are rescaled by a fixed factor of 0.9688, which was chosen based on the data recommended by Merrick et al. [16].

The $G(\nu)$ functions, calculated according to [17] in the one-phonon-approximation, from the time-of-flight IINS spectra of $[Sr(H_2O)_6]Cl_2$ against the wavenumber scale for three temperatures of measurements are shown in Fig. 4. It should be reminded here, that in the $G(\nu)$ spectrum bands associated with all molecular

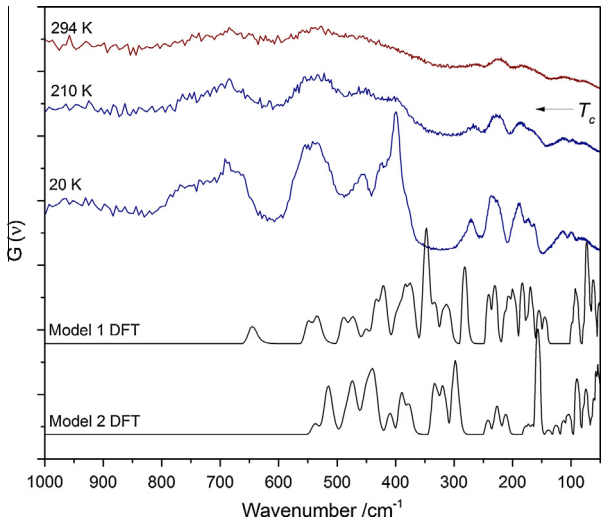

Fig. 4. The temperature dependence of the experimental phonon density of states spectra $G(\nu)$ of $[Sr(H_2O)_6]Cl_2$ and calculated spectrum for isolated equilibrium Models 1 and 2.

vibrations are allowed, because there are no symmetry dependent selection rules such as occurring in optical spectroscopy. One can see that the $G(\nu)$ spectra obtained at 294 K are very diffused, because of a large dynamical disorder of H_2O molecules connected with their fast molecular reorientational motions. The $G(\nu)$ spectra obtained for the low temperature phase at temperatures 20 and 210 K show some separate peaks characteristic for more or less ordered phase. Intensities of particular transitions in IINS spectra depend on atomic mean-square displacement and can be easily calculated. We used aCLIMAX software [18] to determine the intensities of transition obtained from DFT calculations (rescaled by a fixed factor of 0.9688). Next, these intensities (Dirac delta function) were convoluted with a resolution function characteristic for NERA spectrometer and converted to density of states with the help of the RES program [19]. The theoretical spectrum is shown in Fig. 4. The IINS spectroscopy is especially sensitive to hydrogen motion hence the experimental neutron spectrum is practically reproduced by the calculation performed for the isolated cation. The contribution of the Cl^- anion is very small, it can be practically neglected. Overall a good agreement between theoretical and experimental IR, RS and $G(\nu)$ spectra was achieved. However this agreement is better for Model 1 when compared to Model 2. The reason is that Model 1 better approximates real structure despite it is simpler than Model 2.

Small discrepancies between calculated and measured IR, RS and IINS spectra are caused by the simplicity of the assumed models. Calculated bands in the region 4000–1000 cm^{-1} are shifted towards higher wavenumbers with respect to experimental data, whereas the bands in the region 1000–50 cm^{-1} are shifted in the opposite direction (see Figs. 2–4). The hydrogen bond interactions were not taken into account in our calculation and this is the reason why the calculated modes are overestimated. On the other hand our models do not incorporate interaction presented in crystals. Hence, we were not able to calculate frequency of phonons, and additionally reproduced bands in the lower wavenumber region are underestimated. This is caused by neglecting the crystal packing. Using the plane-wave DFT calculation with periodic boundary conditions for a crystalline phase would be a much better approximation. In the region of 3000–1700 cm^{-1} of $[Sr(H_2O)_6]Cl_2$ infrared spectra overtones and combinational bands are observed. Because we have computed normal modes, no bands are predicted theoretically in the mentioned region.

The bands assignments of $[Sr(H_2O)_6]Cl_2$ vibrational spectrum: experimental (IR, RS, IINS) and calculated for Model 1 and Model 2, are given in Table 3. In the present paper all bands present in the calculated vibrational spectra were assigned based on the visualization of the individual normal vibrations. Calculated spectra obtained for the Model 1 and Model 2 can be divided into a few characteristic ranges of the wavenumbers. Below, the results for Model 1 are only presented. In parenthesis are presented the experimental (IR) data. The spectral area below 97 cm^{-1} (95 cm^{-1}) is connected with skeletal bending deformations. The stretching Sr–O mode mixed with librational (twisting $\tau(H_2O)$) modes were localized in frequencies range from 212 to 144 cm^{-1} (223–120 cm^{-1}). At 241 and 230 cm^{-1} wavenumbers (236 cm^{-1}) twisting $\tau(H_2O)$ vibrations of water molecules are present. Vibration observed at 282 cm^{-1} (276 cm^{-1}) can be assigned to rocking $\rho(H_2O)$ of H_2O molecules. In the wavenumbers region: 351–309 cm^{-1} (308 cm^{-1}) the calculated bands were interpreted as wagging $\omega(H_2O)$ and rocking $\rho(H_2O)$ modes. Bands between 398–371 cm^{-1} (non observed) were interpreted as rocking $\rho(H_2O)$ modes of water ligands and between 644 and 419 cm^{-1} (655–394 cm^{-1}) wagging mixed with librational modes are present. For comparison Singh and Khanna [20] have observed in experimental infrared spectrum of $[Sr(H_2O)_6]Cl_2$ the following frequencies of libratory (rocking, wagging, twisting) modes of H_2O molecules: 705, 552, 658 cm^{-1} (bridging type bonding) and 460, 400, 418 cm^{-1} (terminal type bonding). In the vicinity of 1596–1554 cm^{-1} (1654–1628 cm^{-1}) bending δ(HOH) modes are observed. Finally two sets of symmetrical 3649–3593 cm^{-1} (3513–3215 cm^{-1}) and asymmetrical 3728–3706 cm^{-1} (3603 cm^{-1}) stretching OH modes are present. This comparison indicate that there is a quite good qualitative agreement of the calculated spectrum with the experimental one.

Crystal structure identification by neutron powder diffraction

The neutron powder diffraction (NPD) patterns for polycrystalline $[Sr(H_2O)_6]Cl_2$ were registered during sample heating at three temperatures of measurement: 20, 210 and 294 K. Fig. 5 presents the NPD patterns registered at 294 K (phase I) and at 210 and 20 K (phase II) for two scattering angles: (a) $2\theta = 49.90°$ and (b) $2\theta = 62.60°$. Thermal expansion is observed by increasing lattice distances; however, we cannot see any important differences between the NPD patterns obtained for both crystalline phases. This means that the crystal structure of $[Sr(H_2O)_6]Cl_2$ does not change (or the changes are very slight) after the phase transitions, at least as measured by the neutron diffraction method. As was stated above from single crystal measurements, the crystal structure does not change in the phase transition at T_C. This is mainly connected with slight changes in water molecule orientation. This aspect cannot be seen and investigated by means of neutron diffraction for $[Sr(H_2O)_6]Cl_2$ mainly due to high incoherent cross-section scattering for hydrogen atoms, which is why the neutron powder diffraction method is insensitive to water molecule orientation. This conclusion is compatible with the results obtained by us earlier from single crystal X-ray measurements [1]. The bars at the top of Fig. 5 denote d_{hkl} spacing calculated for the crystal structure determined from single X-ray measurements [1]. The NPD patterns can be evaluated only qualitatively. It is not possible to relate structure (an average position or orientation of atoms) with dynamics. However, the patterns provide useful and important results. Of course the deuteration of the sample may provide more structural information. High-quality diffraction studies performed on an isotopically substituted sample can reveal structure information such as deuteron position with high accuracy. However, it should be remembered that in some cases, deuteration can have an influence on investigated physicochemical properties (for

Table 3
Band positions of the $G(\nu)$ (IINS), Raman (FT-RS) and infrared (FT-IR) vibrational spectra of $[Sr(H_2O)_6]Cl_2$ at low temperature phases compared with calculated (DFT) frequencies ν (cm^{-1}) (scaled by 0.9688).

Experimental			DFT calculated		Assignments of vibrations
ν_{IR} (cm^{-1})	ν_{RS} (cm^{-1})	ν_{IINS} (cm^{-1})	Model 1 ν (cm^{-1})	Model 2 ν (cm^{-1})	
			3728	3718	ν_{as}(O–H)
			3727.9	3717.2	
			3725	3716.8	
3603			3721.6	3716.7	
			3721.4	3710	
			3709	3709.7	
			3708	3708.9	
			3707	3708.7	
			3706	3696	
			3648.8	3643.5	ν_s(O–H)
			3648.1	3643.4	
			3644	3611	
			3644	3593	
			3640	3591	
3513			3615	3581.7	
3462			3608	3581.3	
3419	3425		3604	3567.9	
3380			3593	3567.3	
3215	3234				overtones/combinational bands
2424	2426				
2371					
2309	2333				
2154	2136				
2100	2098				
2055					
1878					
1836					
			1596	1605	δ(H–O–H)
			1594	1604.5	
			1589	1583	
			1585	1580	
1654	1655		1572	1572	
1628			1571	1570	
			1564	1568	
			1561	1567	
			1554	1558	
1243					
889					
769	721				
655	644	667	644		ω(H–O–H), ρ(H–O–H)
				536	
				518	
548	566	541	548	512.8	
			533	512.7	
			489	485	
		456	476	478	
			469	471	
394	484	422	450	470.5	
	454	400	435	456	
			431	448	
			422	447	
			419	441	
				435.4	
			398		ρ(H–O–H)
			388		
			380	409	
			371	389	
				376	

Table 3 (*continued*)

Experimental			DFT calculated		Assignments of vibrations
ν_{IR} (cm^{-1})	ν_{RS} (cm^{-1})	ν_{IINS} (cm^{-1})	Model 1 ν (cm^{-1})	Model 2 ν (cm^{-1})	
			351		ω(H–O–H), ρ(H–O–H)
			350		
			347	335	
308			344	332	
			332	322.7	
			318	316	
			309	300	
				299	
276	286	271	282	293	ρ(H–O–H)
236	233	236	241	243	τ(H–O–H)
				242	
			230	229	
				228	
				225	
				224	
				213	
				210	
			212		ν(Sr–O), τ(H–O–H)
			204		
			203		
223	190	189	197		
			196		
			184		
192	184	174	173	177	
166	160	163	168	169	
			167	162	
			155	157	
	134		144	156	
				139	
				126	
120	117	116			
				112	skeletal bending deformations
				104	
95	96	99	97	90	
			92	89	
			89	81	
			76	76	
77		84	72	72	
69			71	62	
			63	59	
			60	54.1	
			51	54.0	
			42.6	50	
			42.2	45	
			37	44.6	
			36	44.4	
			20	34	
				30	
				29	
				18	
				14	

example, the phase transition temperature of the deuterated analogue is often shifted with respect to a 'normal' sample).

Connection between the molecular motions and phase transition

Temperature dependence of the Raman light scattering bands

The shape of Raman light scattering and infrared absorption bands contain information concerning molecular reorientational motions of molecules in condensed phases, then, and only then, when the reorientational correlation time τ_R, which is inversely proportional to the full width at half maximum (FWHM) of the spectral IR and RS bands associated with the internal vibration of the reorienting molecule, is of an order 10^{-13}–10^{-11} s. Fig. 6 presents Raman spectra at selected temperatures.

We follow the analysis of FWHM which is based on the formula used for the damping associated with the order–disorder transition [21,22]. The reorientational correlation time τ_c is the mean time between instantaneous jumps from one potential well to the other, and it is defined by the following formula:

$$\tau_c = \tau_\infty \cdot \exp\left(\frac{E_a}{RT}\right), \quad (2)$$

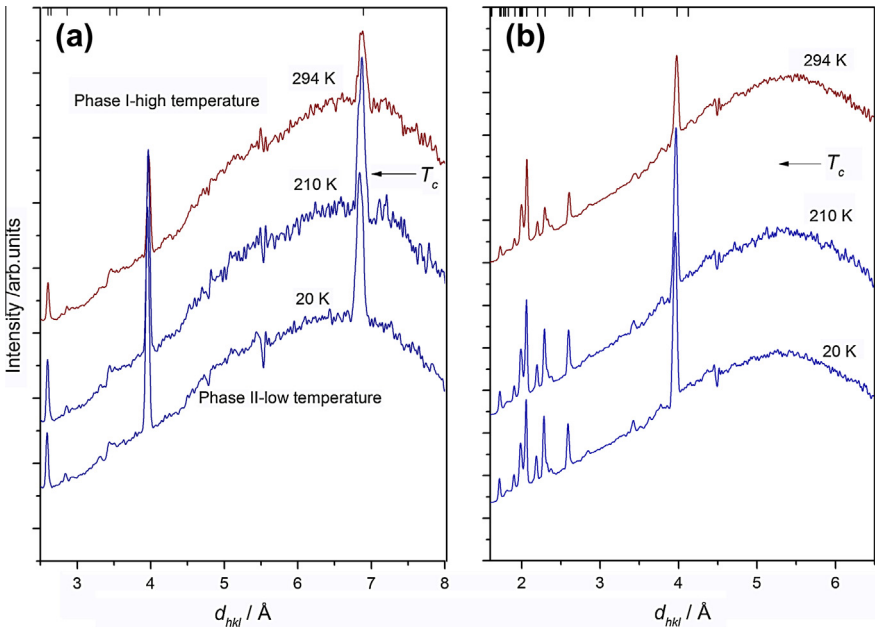

Fig. 5. The NPD patterns of $[Sr(H_2O)_6]Cl_2$ registered upon heating the sample presented for three temperatures of measurement, at scattering angles (a) $2\theta = 49.90°$ and (b) $2\theta = 62.60°$.

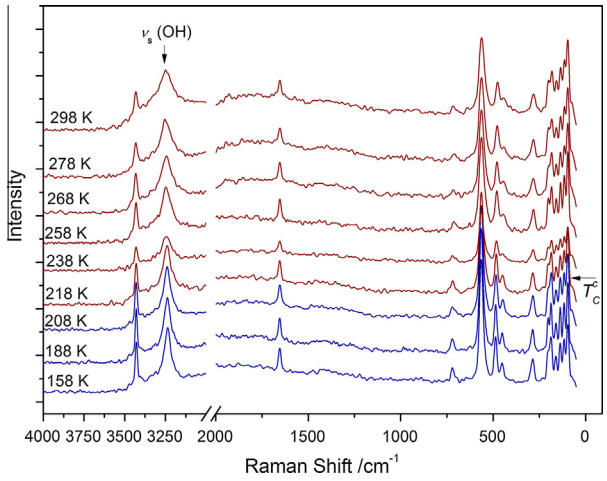

Fig. 6. Raman spectra in the frequency range of 4000–300 cm^{-1} and 2000–50 cm^{-1} at different selected temperatures (during cooling of the $[Sr(H_2O)_6]Cl_2$ sample). Phase transition temperature registered by DSC during cooling is indicated by arrow.

where: τ_∞ is the relaxation time at an infinite temperature T, E_a is the potential barrier height for reorienting groups, $R = N_A \cdot k_B = 8.314472\ J\ K^{-1}mol^{-1}$ is the gas constant, and N_A and k_B are Avogadro's and Boltzmann's constants, respectively. When $\omega^2 \cdot \tau_R^2 \gg 1$, where $\omega = 2\pi\nu$ and ν is the frequency of a particular phonon mode, the temperature dependence of the FWHM of the infrared and Raman bands connected with this mode is determined by following expression [21–23]:

$$\mathrm{FWHM}(T) = (a + bT) + c \cdot \exp\left(-\frac{E_a}{RT}\right), \quad (3)$$

where a, b, c and E_a are fitting parameters. Here the E_a is activation energy of the reorientation process. The linear part of Eq. (3) is associated with the vibrational relaxation and the exponential term is associated with rotational relaxation and corresponds to the thermal reorientational motions of a diffusion nature.

The FWHM of bands related to the selected modes in the FT-MIR and FT-FIR (see Ref. [7]) and Raman spectra obtained at different temperatures were calculated by fitting the Lorentz function using the ORIGIN program to the particular band. We intended to check whether the phase transitions in $[Sr(H_2O)_6]Cl_2$ are related to the reorientational dynamics change of the H_2O ligands. In order to do this, an analysis of the full width at half maximum (FWHM) of some properly chosen bands in Raman scattering spectra vs. temperature was performed. The chosen band for further analysis is connected with the stretching vibration vs(H2O) modes at ca. 3248 cm^{-1} in the RS spectrum. In the high temperature phase we can observe the broadening of these bands, what is very characteristic for orientationally dynamically disordered crystals (ODIC) [24]. Fig. 7(a) presents the temperature dependence of the FWHM of RS bands located at 3248 cm^{-1} connected with the vs(OH) mode. As can be seen, FWHM of this band decreases exponentially during cooling of the sample down to the phase transition region. In the vicinity of the phase transition the FWHM changes discontinuously and below the phase transition it again decreases exponentially. It is worth mentioning that decrease of FWHM in the vicinity is equal to ca. 10 cm^{-1}. The similar drop of the FWHM is observed on further cooling in the temperature range 230–160 K. Eq. (3) fits the solid lines in Fig. 7(a). The fitted parameters are listed in Table 4. Because of limited number of experimental points the fitting was performed for points lying in high and low temperature phase, together. Thus the mean value of activation energy for reorientation of H_2O ligands in the both high and low temperature phase was estimated: $E_a(I/II) = 7.7 \pm 0.4$ kJ mol^{-1}. This is in a good agreement with the data obtained by us from infrared measurements [7].

Fig. 7(b) demonstrates temperature dependence of the peak position of this band. We can see that this dependence is comparable to the corresponding FWHM vs. T dependences presented in Fig. 7(a). This fact suggests that the reorientational motions of H_2O ligands do contribute to the phase transition mechanism.

FT-RS analysis for $[Sr(H_2O)_6]Cl_2$ compound, suggests that the fast H_2O reorientation which take place in the high temperature phase does not stop, and even does not distinctly slowing down, at the phase transitions to the low temperature phase. However, one can observe in the vicinity of T_C a small change of the reorientational dynamics of H_2O molecules.

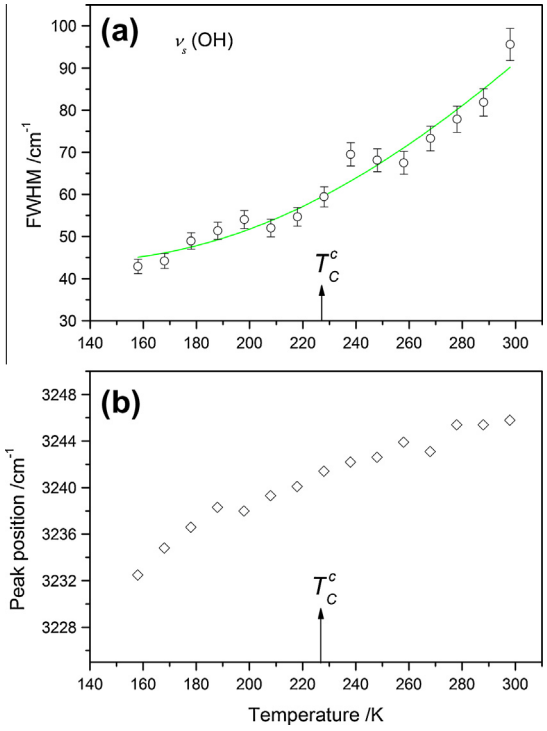

Fig. 7. Temperature dependence of (a) FWHM of Raman band at ~3248 cm^{-1} and (b) peak position in cm^{-1}, associated with the stretching vibration of water molecule $\upsilon_s(H_2O)$ mode. Arrow denotes phase transition temperature registered by DSC at cooling of the $[Sr(H_2O)_6]Cl_2$ sample. Solid lines represent fitting of Eq. (3) to all experimental points.

Table 4
The fitted parameters: *a*, *b*, *c* and E_a for the temperature dependence of FWHM of the infrared band at ~3248 cm^{-1} associated with ν_s(OH) mode obtained in the temperature range 298–158 K of $[Sr(H_2O)_6]Cl_2$.

Fitting parameters	Phase I and II
$[Sr(H_2O)_6]Cl_2$ analysed IR band at ~3248 cm^{-1}; ν_s(OH) mode	
a (cm^{-1})	48.0 ± 0.1
b (cm^{-1} K^{-1})	−0.040 ± 0.008
c (cm^{-1})	1215.4 ± 501.8
E_a (kJ mol^{-1})	7.7 ± 0.4

Similar values of activation energy for 180° jumps of H_2O around M–O bond, namely: E_a(I/II) = 4.9 kJ mol^{-1} and E_a(I/II) = 5.4 kJ mol^{-1}, were obtained from the RS and IR measurements for $[Ba(H_2O)_3](ClO_4)_2$ [25], respectively. Such rather small energy activation values suggest that the hydrogen bonds are weak [26,27].

Incoherent neutron scattering spectra vs. temperature

The time-of-flight IINS/QENS spectra of $[Sr(H_2O)_6]Cl_2$ as a function of neutron wavelength, obtained simultaneously with the NPD patterns at three different temperatures are presented in Fig. 8. The IINS spectra obtained at 294 K are very diffuse because of a large dynamical disorder connected with the fast molecular reorientations, especially of H_2O molecules.

The elastic peak (measured simultaneously with IINS spectra and normalised to the same intensity) presented in Fig. 8 was summed up from 15 detectors. Of course, such an approach does not allow for a detailed discussion of the geometry of the motion (EISF dependency on neutron momentum transfer Q) but is justified because the correlation time (inversely proportional to quasi-elastic broadening) does not depend on Q. The elastic peak

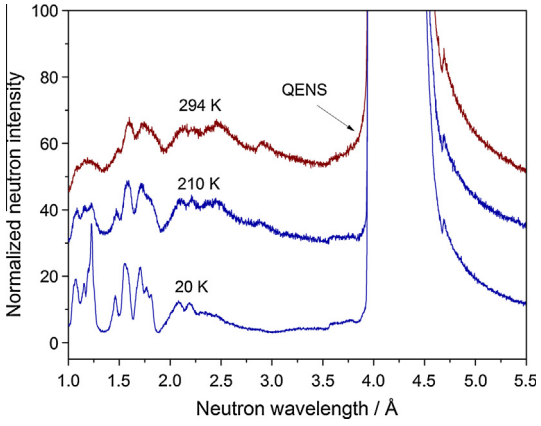

Fig. 8. The temperature dependence of the IINS spectra of $[Sr(H_2O)_6]Cl_2$ normalised to the same intensity.

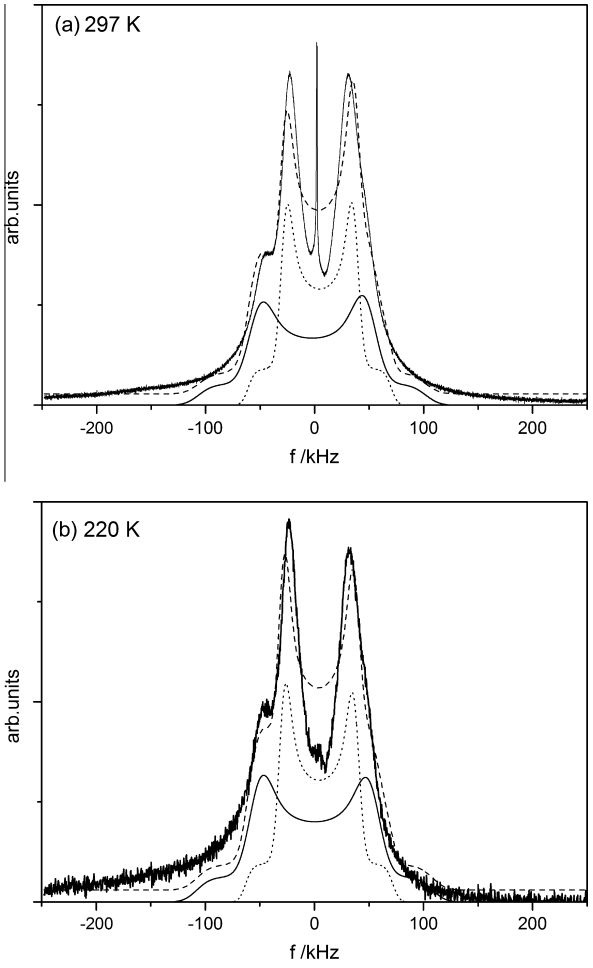

Fig. 9. ^{1}H NMR spectrum of $[Sr(H_2O)_6]Cl_2$ polycrystalline powder recorded at (a) 297 K and at (b) 220 K. The spectrum can be decomposed onto two Pake doublets. Bold solid line: experimental data, dashed line: fitted sum of two Pake doublets, the first one coming from water (1), dotted line, and the second one coming from water (2), thin solid line.

registered at 20 K and at 210 K (below phase transition) shows no broadening. Taking into account the energy resolution of the NERA spectrometer, this implies that protons from H_2O ligands do not perform fast (correlation time 10^{-12}–10^{-13} s) reorientations. We found that when the sample was heated to 294 K (above

phase transition) small QENS broadening appeared in the spectrum. We suspect that this broadening is connected with picosecond reorientational 180° jumps of H_2O molecules around their twofold symmetry axis. This is a natural consequence of thermal activation of the motion of water molecules. At higher temperatures the motion of H_2O ligands begins, with correlation time of the order 10^{-12}–10^{-13} s. The lack of such broadening below T_C confirms that at this phase transition the H_2O ligands suddenly change (slowing down) the rate of their reorientational jumps.

Proton magnetic resonance

^{1}H NMR spectra vs. temperature

The ^{1}H NMR spectra of hexaaquastrontium chloride, $[Sr(H_2O)_6]Cl_2$, solid polycrystalline powder, recorded at room temperature (297 K) and at 220 K were shown in Fig. 9a and b. The spectra are broadened by the dipole–dipole interaction of spin pairs and reveal the pattern of the Pake doublet for solid isotropic powder [28,29]. The observed line may be decomposed onto two Pake doublets differentiated by a dipolar broadening, namely one with the splitting of the line $2a = (67.3 \pm 2.3)$ kHz, named water (1) and the second with the effective line splitting $2a = (110 \pm 3)$ kHz, named water (2), where a is defined as follows:

$$a = \frac{3}{2}\frac{\mu_0}{4\pi}\frac{\gamma_H^2\hbar}{r^3}, \tag{4}$$

where γ_H is the magnetogyric ratio of the proton and r is the distance between the pair of two relaxing protons.

The Pake doublet is defined as follows [28,30]. The line intensity, $G_P(f)$, is a sum of two components:

$$G_P(f) = C(G_1(f) + G_2(f)), \tag{5}$$

where $G_1(f) = (a+f)^{-1/2}$ in the range $-a < f < 2a$, and $G_1(f) = 0$ elsewhere and $G_2(f) = (a-f)^{-1/2}$ in the range $-2a < f < a$, and $G_2(f) = 0$ elsewhere. C is the scaling constant.

Experimental data was fitted with a sum of two doublets convoluted with Gaussian profile (average full width at half maximum of the Gaussian line was equal to 12.2 kHz and 21.2 kHz for doublet one and two, respectively). For higher temperatures, beside two solid line components, fitted well by Pake doublets, a narrow line was detected in the central part of spectrum. This line probably comes from water loosely bound on the surfaces of crystallites (with the halfwidth equal to 800–1700 Hz increasing with the temperature decrease). The narrow line component was not detected for the temperatures below 250 K.

The temperature dependency of proton spin–lattice relaxation time T_1

Magnetization recovery curves were constructed from the area under each doublet plotted vs. the delay time τ. An exponential function (Eq. (6)) was fitted to the data to obtain the spin–lattice relaxation time, T_1, for a given line component:

$$M_z(\tau) = M_0\left[1 - 2\exp\left(-\frac{\tau}{T_1}\right)\right]. \tag{6}$$

In case of dipolar spin–lattice relaxation between like spins the dependency of the spin–lattice relaxation time, T_1, and correlation time of the molecular motions τ_c is given by [31,32]:

$$\frac{1}{T_1} = \frac{3}{10}\left(\frac{\mu_0}{4\pi}\right)^2\frac{\gamma^4\hbar^2}{r_{ij}^6}\left(\frac{\tau_c}{1+\omega^2\tau_c^2} + \frac{4\tau_c}{1+4\omega^2\tau_c^2}\right), \tag{7}$$

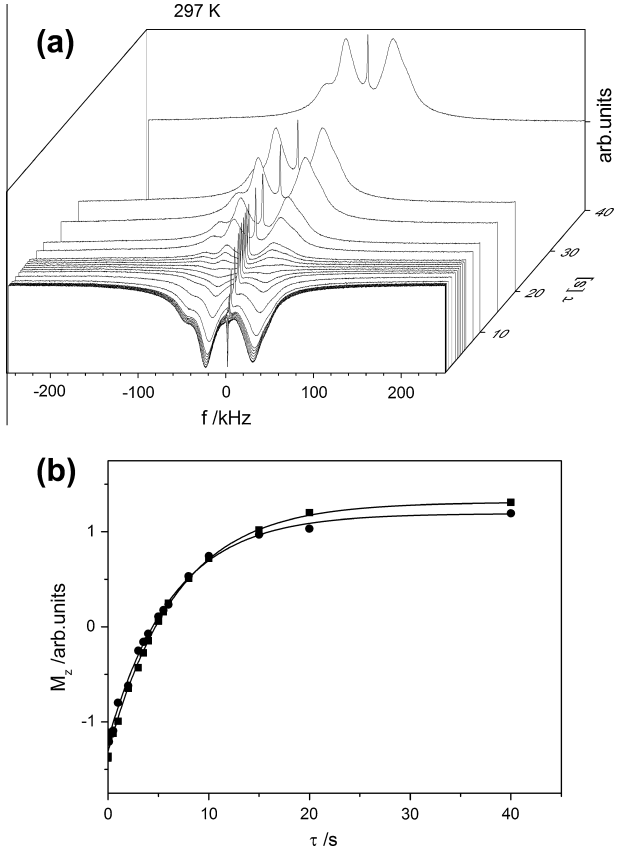

Fig. 10. ^{1}H NMR relaxation spectroscopy experiment for solid polycrystalline $[Sr(H_2O)_6]Cl_2$ powder detected at 297 K (a) stacked plot of the spectra. The narrow line comes from free water accidentally bound on the surfaces of the crystallites; (b) magnetization recovery curve for two Pake doublets (solid squares: water '1', solid dots: water '2', solid line: one exponential function fitted (Eq. (6)).

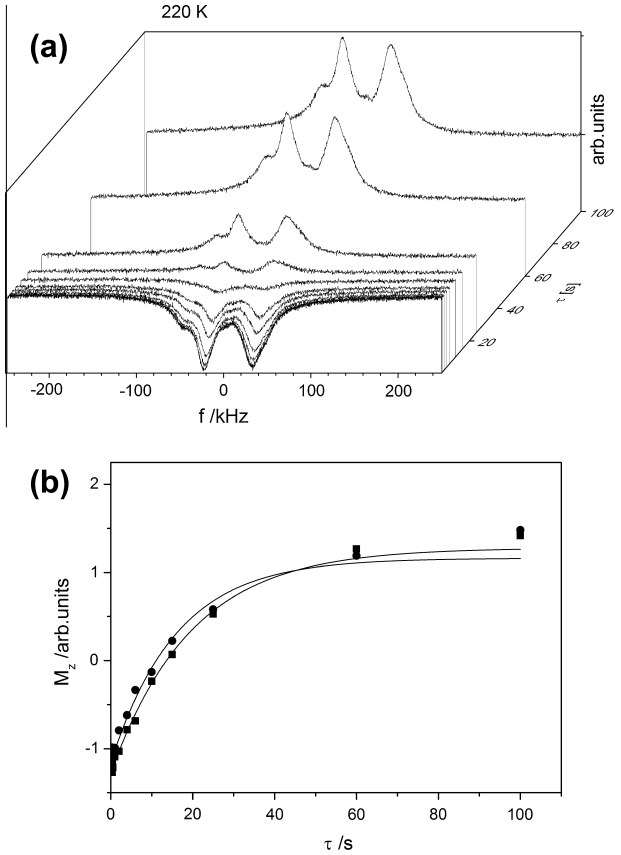

Fig. 11. ^{1}H NMR relaxation spectroscopy experiment for solid polycrystalline $[Sr(H_2O)_6]Cl_2$ powder detected at 220 K (a) stacked plot of the spectra; (b) magnetization recovery curve for two Pake doublets (solid squares: water (1), solid dots: water (2), solid line: one exponential function fitted (Eq. (6)).

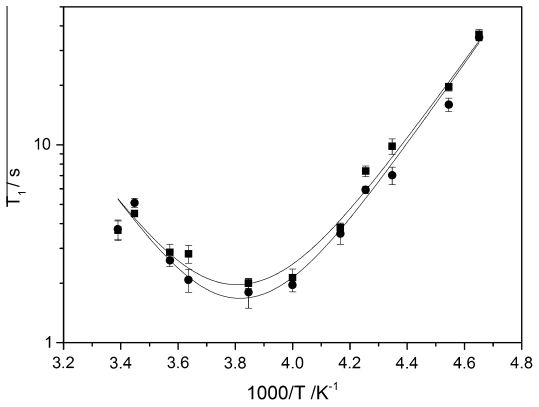

Fig. 12. The Arrhenius plot of the longitudinal relaxation time, T_1, temperature dependency for solid polycrystalline $[Sr(H_2O)_6]Cl_2$ powder (solid squares: water (1), solid dots: water (2), solid line: a fit of the BPP model (Eqs. (7) and (2)).

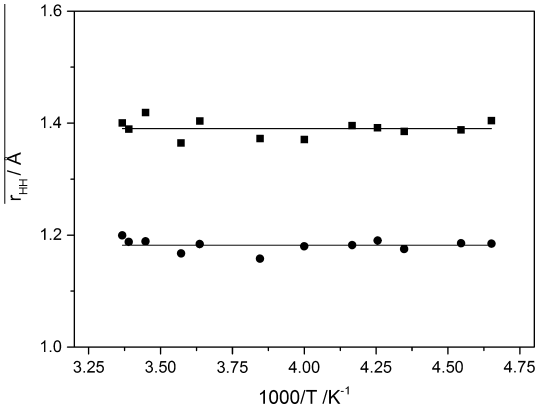

Fig. 13. The distances between dipolar coupled protons in solid polycrystalline $[Sr(H_2O)_6]Cl_2$ powder as calculated from both Pake doublets fitted, solid squares: water (1), solid dots: water (2), solid lines: linear fit (see text).

where r_{ij} is the distance between the pair of interacting spins, and ω the resonant frequency.

Figs. 10a and 11a present ^1H NMR relaxation spectroscopy experiment results for polycrystalline $[Sr(H_2O)_6]Cl_2$ detected at 297 and 220 K, respectively, stacked plot of the spectra. The narrow line comes from free water accidentally bound on the surfaces of the crystallites. Figs. 10b and 11b present for these two experiments the magnetization recovery curve for two "Pake doublets" (solid squares: water (1), solid dots: water (2), solid line: one exponential function fitted (Eq. (6)).

If one assumes that molecular reorientations may be approximated by jumps over the energy barrier, E_a, between two equal energy minima, according to Arrhenius model, the temperature dependence of the correlation time, τ_c, may be expressed by Eq. (2). Fig. 12 shows the Arrhenius plot of T_1 vs. $1000/T$ for solid polycrystalline $[Sr(H_2O)_6]Cl_2$ sample. The BPP dependence fits well the T_1 temperature dependency. Activation energies fitted are: E_a (1) = (38.8 ± 5.0) kJ mole^{-1} for water (1) and E_a (2) = (40.0 ± 4.1) kJ mole^{-1} for water (2), respectively. For the analysed temperature range, longitudinal relaxation time is the shortest for 262 and 261 K for line 1 and 2, respectively. Knowing that T_1 has a minimum for $\omega \cdot \tau_C = 0.616$ [32], a correlation time for minimum for both Pake doublets is: $\tau_c = 3.3 \cdot 10^{-10}$ s.

Average distances between the interacting protons calculated from the linear fit (Eqs. (4) and (5)) in both Pake doublets (see Fig. 13) fitted are: for water (1) protons: $r_{ij}^1 = (1.390 \pm 0.005)$ Å, for water (2) protons: $r_{ij}^2 = (1.182 \pm 0.003)$ Å. Fig. 14 shows the area under doublet 1 expressed in units of total area of both signals $A_1/(A_1 + A_2)$ with a fitted line. A ratio of the areas of first doublet and the total signal was acquired by fitting a line and it was equal 0.50 ± 0.02.

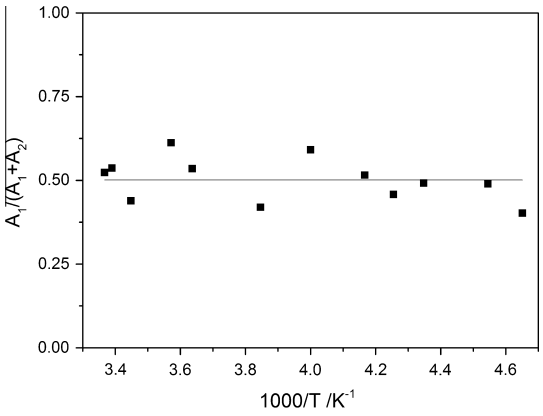

Fig. 14. Area under doublet 1 expressed in units of total area of both signals $A_1/(A_1 + A_2)$ with a fitted line.

Conclusions

1. The neutron diffraction pattern for $[Sr(H_2O)_6]Cl_2$ at 294 K is nearly exactly the same as that at 210 K, which implies that the phase transition at $T_C^h = 252.9$ K (on heating) and at $T_C^c = 226.5$ K (on cooling) does not display a structural character. The space group (P321, No. = 150) is the same for the high and low temperature phases.
2. Optical spectra calculated by the DFT method (B3LYP functional, LANL2DZ ECP basis set (on Sr atom) and 6-311 + G(d,p) basis set (on H and O atoms) for the isolated $[Sr(H_2O)_9]^{2+}$ cation show close agreement with the experimental spectra IR, RS and phonon density function spectra.
3. From the temperature dependence of FWHM of the band connected with ν_s(OH) mode in Raman spectra, we can conclude that the reorientational motions of H_2O ligands are disturbed at the phase transition. The ligands perform fast ($\tau_R \approx 10^{-11}$–10^{-13} s) stochastic reorientational motions in the low and in the high-temperature phase of the title compound. However, small drop of FWHM in the vicinity of PT is observed. The estimated mean value of activation energies for reorientation of the H_2O ligands is equal to ca. 8 kJ mol^{-1}.
4. The QENS data registered at 20 K and 210 K does not show any broadening. This implies, taking into account the resolution of the NERA spectrometer, that the reorientational correlation time τ_c of water ligands is longer than 10^{-12}–10^{-11} s. However, at the high temperature phase, quasielastic broadening is clearly visible, what implies that H_2O ligands start to perform fast ($\tau_c \approx 10^{-12}$–10^{-13} s) reorientational motion.
5. ^1H NMR measurements indicated that there are two type of the water molecules in the crystal lattice of $[Sr(H_2O)_6]Cl_2$, which are structurally not equivalent average distances between the interacting protons are: 1.39 and 1.18 Å. However, reorientational dynamics of these both types H_2O molecules is very similar ($\tau_c = 3.3 \cdot 10^{-10}$ s and $E_a \approx 40$ kJ mole^{-1}).
6. Confrontation of the results obtained by optic (RS, IR) and neutron (QENS) spectroscopy methods, on the one hand, with those obtained by ^1H NMR, on the other hand, indicate clearly that there exists at least two kinds of H_2O molecules in $[Sr(H_2O)_6]Cl_2$ crystal lattice with quite different reorientational dynamics.

Acknowledgements

The research was carried out with the equipment (FT-IR and NMR spectrometers) purchased thanks to the financial support of the European Regional Development Fund in the framework of the Polish Innovation Economy Operational Program (contract no. POIG.02.01.00-12-023/08). This research was also supported in part by PL-Grid Infrastructure.

References

[1] P.A. Agron, W.R. Busing, Acta Crystallogr. C 42 (1986) 141.
[2] R.B. English, L.R. Nassimbeni, Acta Crystallogr. C 40 (1984) 580.
[3] A.T. Jensen, K. Dan, Vidensk. Selsk. Mat. Fys. Medd. 9 (1940) 3.
[4] A. Leclaire, M.M. Borel, Acta Crystallogr. B33 (1977) 2938.
[5] D.M. Adams, W.R. Trumble, J. Chem. Spc. Faraday Trans. II 70 (1967) 1974.
[6] B. Singh, S.P. Gupta, B.N. Khanna, Proc. Nucl. Phys. Solid State Phys. Symp. 21C (1978) 333.
[7] J. Hetmańczyk, Ł. Hetmańczyk, A. Migdał-Mikuli, E. Mikuli, Spectrochim. Acta A 115 (2013) 504.
[8] I. Natkaniec, S.I. Bragin, J. Brańkowski, J. Mayer, in: U. Steigenberger, T. Brome, G. Rees, A. Soper, (Eds.); Proceedings of the ICANS XII Meeting, Abingdon 1993, RAL Report 94-025, vol. I, 1994, pp. 89.
[9] M.J. Frisch, G.W. Trucks, H.B. Schlegel, G.E. Scuseria, M.A. Robb, J.R. Cheeseman, J.A. Montgomery, Jr., T. Vreven, K.N. Kudin, J.C. Burant, J.M. Millam, S.S. Iyengar, J. Tomasi, V. Barone, B. Mennucci, M. Cossi, G. Scalmani, N. Rega, G.A. Petersson, H. Nakatsuji, M. Hada, M. Ehara, K. Toyota, R. Fukuda, J. Hasegawa, M. Ishida, T. Nakajima, Y. Honda, O. Kitao, H. Nakai, M. Klene, X. Li, J.E. Knox, H.P. Hratchian, J.B. Cross, V. Bakken, C. Adamo, J. Jaramillo, R. Gomperts, R.E. Stratmann, O. Yazyev, A.J. Austin, R. Cammi, C. Pomelli, J.W. Ochterski, P.Y. Ayala, K. Morokuma, G.A. Voth, P. Salvador, J.J. Dannenberg, V.G. Zakrzewski, S. Dapprich, A.D. Daniels, M.C. Strain, O. Farkas, D.K. Malick, A.D. Rabuck, K. Raghavachari, J.B. Foresman, J. V. Ortiz, Q. Cui, A.G. Baboul, S. Clifford, J. Cioslowski, B.B. Stefanov, G. Liu, A. Liashenko, P. Piskorz, I. Komaromi, R.L. Martin, D.J. Fox, T. Keith, M.A. Al-Laham, C.Y. Peng, A. Nanayakkara, M. Challacombe, P.M.W. Gill, B. Johnson, W. Chen, M.W. Wong, C. Gonzalez, J.A. Pople, Gaussian 03, Revision D.01, Gaussian Inc, Wallingford CT, 2004.
[10] A.D. Becke, J. Chem. Phys. 98 (1983) 5648.
[11] P.J. Stephens, F.J. Devlin, C.F. Chabalowski, M.J. Frisch, J. Phys. Chem. 98 (1994) 11623.
[12] L.E. Roy, P.J. Hay, R.L. Martin, J. Chem. Theory Comput. 4 (2008) 1029.
[13] K.T. Schuchardt, B.T. Didier, T. Elsethagen, L. Sun, V. Gurumoorthi, J. Chase, J. Li, T.L. Windus, J. Chem. Inf. Model 47 (2007) 1045.
[14] D. Michalska, R. Wysokinski, Chem. Phys. Lett. 403 (2005) 211.
[15] S.P. Gupta, Y. Kumar, B.N. Khanna, Pramana 36 (1991) 151.
[16] J.P. Merrick, D. Moran, L. Radom, J. Phys. Chem. 111 (2007) 11683.
[17] S.W. Lovesey, Theory of Neutron Scattering from Condensed Matter, Clarendon Press, Oxford, 1984.
[18] A.J. Ramirez-Cuesta, Comput. Phys. Comm. 157 (2004) 226.
[19] W.J. Kazimirov, I. Natkaniec, Preprint P14-2003-48 JINR, Dubna, 2003.
[20] B. Singh, B.N. Khanna, Spectrochim. Acta A 42 (1986) 181.
[21] C. Carabatos-Nédelec, P. Becker, J. Raman Spectrosc. 28 (1997) 663.
[22] P.da R. Andrade, A.D. Pasad Rao, R.S. Katiyar, S.P.S. Porto, Solid St. Commun. 12 (1973) 847.
[23] P.da R. Andrade, S.P.S. Porto, Solid St. Commun. 13 (1973) 1249.
[24] Dynamics of Solids and Liquids by Neutron Scattering in: S.W. Lovesey, T. Springer (Eds.), Topics in Current Physics, vol. 3, Springer-Verlag, Berlin, 1977.
[25] J. Hetmańczyk, Ł. Hetmańczyk, A. Migdał-Mikuli, E. Mikuli, A. Wesełucha-Birczyńska, J. Raman Spectrosc. 43 (2012) 1118.
[26] C. Nöldeke, B. Asmussen, W. Press, H. Buttner, G. Kearley, R.E. Lehner, B. Ruffle, J. Chem. Phys. 113 (2000) 3219.
[27] C. Nöldeke, B. Asmussen, W. Press, H. Buttner, G. Kearley, Chem. Phys. 289 (2003) 275.
[28] G.E. Pake, Solid State Physics. Advances in Research and Applications, vol. 2, Academic Press Inc., New York, 1956, p. 1.
[29] V.J. McBrierty, K.J. Packer, Nuclear Magnetic Resonance in Solid Polymers, Cambridge University Press, 2006.
[30] G.E. Pake, J. Chem. Phys. 16 (1948) 327.
[31] N. Bloembergen, E.M. Purcell, R.V. Pound, Phys. Rev. 73 (1948) 679.
[32] A.A. Abragam, The Principles of Nuclear Magnetism, Clarendon Press, Oxford, 1961.